Molecular Biology of the Cell
Vol. 21, 2241–2256, July 1, 2010

Rapid Lytic Granule Convergence to the MTOC in Natural Killer Cells Is Dependent on Dynein But Not Cytolytic Commitment

Ashley N. Mentlik,* Keri B. Sanborn,* Erika L. Holzbaur,† and Jordan S. Orange*

Departments of *Pediatrics and †Physiology, University of Pennsylvania School of Medicine, Philadelphia, PA 19104

Submitted November 5, 2009; Revised April 16, 2010; Accepted April 27, 2010
Monitoring Editor: Thomas F.J. Martin

Natural killer cells are lymphocytes specialized to participate in host defense through their innate ability to mediate cytotoxicity by secreting the contents of preformed secretory lysosomes (lytic granules) directly onto a target cell. This form of directed secretion requires the formation of an immunological synapse and occurs stepwise with actin reorganization preceding microtubule-organizing center (MTOC) polarization to the synapse. Because MTOC polarization to the synapse is required for polarization of lytic granules, we attempted to define their interrelationship. We found that compared with the time required for MTOC polarization, lytic granules converged to the MTOC rapidly. The MTOC-directed movement of lytic granules was independent of actin and microtubule reorganization, dependent on dynein motor function, occurred before MTOC polarization, and did not require a commitment to cytotoxicity. This defines a novel paradigm for rapid MTOC-directed transport as a prerequisite for directed secretion, one that may prepare, but not commit cells for precision secretory function.

INTRODUCTION

Natural killer (NK) cells are lymphocytes of the innate immune system capable of killing stressed or infected cells by secreting lytic effector molecules through an immunological synapse (IS) at the interface with the target cell. The NK cell IS forms and functions in a stepwise progression (Orange *et al.*, 2003; Wulfing *et al.*, 2003; Orange, 2008). A major objective of this process is the polarization of lytic granules, a form of secretory lysosome containing the pore-forming molecule perforin, toward the target cell so that their contents can be released. Cytoskeletal reorganization is necessary for maturation of the NK cell IS as F-actin accumulates at the IS and is required for reorientation of the MTOC (Orange *et al.*, 2003; Wulfing *et al.*, 2003). The microtubule network is ultimately responsible for delivery of lytic granules to the IS, and the MTOC is required for their approximating the cytotoxic cell membrane at the IS (Katz *et al.*, 1982; Stinchcombe *et al.*, 2006; Banerjee *et al.*, 2007). In NK cells, precision in directed secretion of lytic granules enables destruction of specific target cells without harming neighboring cells within a complex environment.

Several receptor systems have been characterized for their ability to participate in IS formation and granule polarization. The LFA-1 integrin is required for target cell adhesion and directed secretion through early signaling that initiates actin rearrangements and enables granule focusing to the IS (Barber *et al.*, 2004; Liu *et al.*, 2009). Engagement of more specialized NK cell–triggering receptors such as NKp30, or CD28 on some NK cell lines and subsets, is critical for full NK cell activation and cytotoxicity (Pende *et al.*, 1999; Chen *et al.*, 2006). The activity of triggering receptors includes induction of MTOC polarization to the signaling platform, which facilitates lytic granules joining the synaptic membrane (Vyas *et al.*, 2001; Bryceson *et al.*, 2005; Chen *et al.*, 2006). Several direct activation–induced requirements for MTOC polarization in cytotoxic lymphocytes have been identified (Stinchcombe *et al.*, 2006; Banerjee *et al.*, 2007; Gomez *et al.*, 2007). Thus far, all microtubule-directed events required for lytic granule polarization to the IS, however, are dependent on some prerequisite actin-dependent function.

Once lytic granules polarize to the IS, the actin motor myosin IIA facilitates lytic granule transit through the F-actin–rich NK cell IS (Andzelm *et al.*, 2007; Sanborn *et al.*, 2009). Although plus ends of microtubules insert into the F-actin network at the IS, there has not been any demonstrated requirement for plus-ended lytic granule movement in approximating lytic granules to the synaptic membrane. Instead, lytic granules in association with the MTOC have been defined as the only prerequisite (Stinchcombe *et al.*, 2006; Jenkins *et al.*, 2009). Although a plus-ended motor for lytic granule movement along microtubules in cytotoxic cells has been identified (Burkhardt *et al.*, 1993), presumably the approximation of lytic granules to the MTOC requires minus-end–directed traffic at some point. A specific motor required for, or detailed kinetics of MTOC-directed traffic of lytic granules in cytotoxic cells has not been defined. Analogies in other cell systems in which minus-ended organelle traffic along microtubules occurs similarly to enable directed secretion have also not been identified.

This article was published online ahead of print in *MBoC in Press* (http://www.molbiolcell.org/cgi/doi/10.1091/mbc.E09–11–0930) on May 5, 2010.

Address correspondence to: Jordan S. Orange (Orange@upenn.edu).

Abbreviations used: AWD, area-weighted distance; CTL, cytotoxic T lymphocyte; DIC, differential interference contrast; eNK, ex vivo NK; IS, immunological synapse; LFA-1, leukocyte function-associated antigen 1; MGD, MTOC to granule distance; MTOC, microtubule organizing center; NK, natural killer.

Given that NK cells function in innate immunity, having multiple defined points of regulation is useful in controlling the lethal function of directed secretion for cytotoxicity. Thus, we evaluated the kinetic relationship between the lytic granules, the MTOC, and the IS in NK cells. We found that lytic granule traffic to the MTOC was rapid, occurring long before MTOC polarization to the IS. We have defined this movement as convergence relative to the MTOC, which is meant to indicate that lytic granules amass in close proximity to the MTOC. This rapid minus-end–directed lytic granule movement and convergence was independent of a commitment to cytotoxicity and occurred independently of microtubule and F-actin reorganization. We also defined the minus-end–directed motor used by lytic granules as dynein and found that traffic of lytic granules to the MTOC was required for IS maturation. We propose that rapid lytic granule convergence to the MTOC defines a new checkpoint in cytotoxicity whereby an NK cell prepares for cytotoxicity upon adhesion to a target cell but requires additional activation signaling to polarize this now fully armed lytic machinery. It also defines a new paradigm in organelle traffic for directed secretion, one in which cargoes are compacted to the MTOC to enable efficiency and precision in delivery.

MATERIALS AND METHODS

NK Cell Lines, Target Cell Lines, and Ex Vivo NK Cells

The immortalized NK cell lines YTS and NK92 were used as model NK cell systems. YTS cells were retrovirally transduced with a green fluorescent protein (GFP)-α-tubulin expression construct and sorted by flow cytometry for uniform stable expression as described (Banerjee *et al.*, 2007). The NK92 GFP-α-tubulin–expressing cell line was the kind gift of Dr. Kerry Campbell (Fox Chase Cancer Center). 721.221 and K562 cell lines were used as susceptible target cells for YTS and NK92 cells, respectively, and K562 cells were used as a nonsusceptible target cells for YTS cells. Cell lines were maintained as previously described (Banerjee *et al.*, 2007).

Whole blood was obtained from volunteer donors and was used to prepare ex vivo NK (eNK) cells by negative depletion using the human NK cell isolation kit (Miltenyi Biotec, Auburn, CA) or the RosetteSep human NK cell isolation reagent (StemCell Technologies, Vancouver, BC, Canada). All human samples were obtained after informed donor consent and were used with approval of the institutional internal review board for the protection of human subjects of the Children's Hospital of Philadelphia.

Live Cell Confocal Microscopy

For MTOC polarization studies, GFP-tubulin–expressing cells were suspended in media at a concentration of 3×10^6 cells/ml, incubated with 30 μM LysoTracker Red DND-99 (Molecular Probes, Eugene, OR) for 30 min at 37°C, washed, and resuspended in media at 3×10^6 cells/ml. 721.221 or K562 cells were suspended in media at a concentration of 4×10^5 cells/ml and adhered for 30 min at 37°C to ΔT dishes (Bioptechs, Butler, PA) precoated with antibodies against CD48 (Becton, Dickinson [BD], San Jose, CA) or CD58 (BD), respectively, after which NK cells were added. Conjugates were imaged in a single *z*-axis plane using an Olympus IX-81 DSU spinning disk confocal microscope (Melville, NY) outfitted with a Hamamatsu EM-CCD, C9100-02 camera (Bridgewater, NJ) and Olympus PlanApo N oil immersion, 60×, 1.45 NA objective (Melville, NY) every 10–15 s over 10–40 min. In some experiments a Zeiss Axio Observer Z1 (Thornwood, NY) outfitted with Yokogawa CSU10 spinning disk (Tokyo, Japan), Hamamatsu Orca-AG camera, and Zeiss 63× 1.43 NA oil immersion objective was used. A major difference between the two systems was that the Olympus system used an Olympus halogen illumination system with narrow bandpass filters (Chroma, Brattleboro, VT), whereas the Zeiss system utilized solid state 488-nm (Melles Griot) and 561-nm (Crystal Technology, Palo Alto, CA) lasers managed through a LMM5 laser combiner unit (Applied Spectral Imaging, Carlsbad, CA). In experiments without target cells, LysoTracker-loaded NK cells were added to ΔT dishes precoated with antibodies against CD28 (BD), CD11a (BD), CD45 (BD), or NKp30 (Beckman Coulter, Fullerton, CA) and imaged in a single *z*-axis plane at intervals ranging from 1 to 10 s. In experiments evaluating the role of LFA-1, a previously described murine IgG1 anti-CD11a mAb (clone TS1/22, ATCC; Sanchez-Madrid *et al.*, 1982), or murine IgG1 control mAb (clone MOPC21, BD) were added to NK cells (22.5 μg/ml final concentration) before their addition to target cells. The TS1/22 was used as a highly purified IgG derived from hybridoma culture supernatant. In all live cell experiments temperature was maintained at 37°C using ΔT dish and objective environmental control units (Bioptechs).

Fixed Cell Microscopy

YTS cells alone, or conjugated to 721.221 target cells at a ratio of 2:1 for 0 min and 25 min were adhered to poly-L-lysine–coated glass slides (PolyPrep; Sigma-Aldrich, St. Louis, MO) for 5 min at 37°C. Fixing, permeabilization, and staining were performed as described (Banerjee *et al.*, 2007), except the following reagents were used in the specified sequence: 1) polyclonal rabbit anti-dynein heavy chain (Santa Cruz Biotechnology, Santa Cruz, CA), or anti-pericentrin (rabbit, Abcam, Cambridge, MA), or preimmune rabbit IgG (Sigma-Aldrich); 2) AlexaFluor 568–conjugated goat-anti-rabbit (Invitrogen, Carlsbad, CA), or AlexaFluor 647–conjugated goat anti-rabbit (Invitrogen); 3) biotinylated monoclonal mouse anti-tubulin (Molecular Probes) or biotinylated mouse IgG control (BD); 4) streptavidin-Pacific Blue (Molecular Probes); 5) fluorescein isothiocyanate (FITC)-conjugated mouse anti-perforin clone ΔG9 or FITC-conjugated mouse IgG control (BD). Slides were covered with 0.15-mm coverslips (VWR Scientific, West Chester, PA) using ProLong Gold mounting medium (Molecular Probes). Imaging was acquired using the same microscope, camera, and objective as in live cell imaging.

Image Analysis

Image sequences were analyzed using Volocity software (Improvision, Lexington, MA), and images for presentation were contrast-enhanced uniformly using Adobe Photoshop (San Jose, CA). For analysis, unadjusted images were evaluated in Volocity for fluorescence corresponding to the MTOC (GFP maximal intensity), or lytic granules (LysoTracker Red maximal intensity) was selected based on 2–5 SD above mean intensity. In time-lapse experiments, one in four images was utilized for quantitative analysis, whereas in streaming video experiments, all were used. To measure MTOC polarization, a line connecting the MTOC to the center of the IS was obtained over time using Volocity software. To measure granule convergence to the MTOC, *x* and *y* coordinates of the MTOC and all lytic granule regions in the plane of the MTOC were obtained. The length of the shortest line connecting the MTOC and each granule region was calculated as if it were the hypotenuse of the triangular region defined by the individual object coordinates, thus representing the MTOC-to-granule distance (MGD). The MGD was determined for each lytic granule region present in an individual image from a single time point, and mean MGD was determined. Thus, the MGD was calculated using Equation 1:

$$\mathrm{MGD} = \frac{\left(\sum_{i=1}^{n} \sqrt{(x - x_i)^2 + (y - y_i)^2}\right)}{n} \quad (1)$$

where x and y were the coordinates of the MTOC centroid and x_i and y_i were the coordinates of the centroid of an individual lytic granule region.

Where specified, the mean MGD over all time points recorded was averaged to provide an estimate of the distances throughout the entire observation of the cell. In experiments where cells did not contain a GFP-tubulin construct (Figure 9) the *x, y* coordinates of the centroid of the entire region outlined by all lytic granules within the cell was determined and used instead of the MTOC to provide a measure of proximity of lytic granule regions.

To account for any differences in the area of individual lytic granule regions in a single *z*-axis plane, which could bias the MGD away from the actual mean distance of all lytic granules from the MTOC, a modified use of Shepard's Method was applied. This was considered important as clusters of lytic granules could inappropriately be discerned as an individual granule, therefore inappropriately considering the number of granules at a particular distance from the MTOC. This modification allowed weighting of the distances by the area of the lytic granule regions and was noted as the area-weighted distance (AWD; Equation 2):

$$\mathrm{AWD} = \sum_{i=1}^{n} \mathrm{MGD}_i * \left[\frac{A_i}{\sum_{i=1}^{n} A}\right] \quad (2)$$

where A_i is the area of the lytic granule region being measured, A is the total lytic granule area in that particular image, and MGD_i is the MGD for the lytic granule region A_i. Because the lytic granule region weighted area was normalized to the total present in each plane, measured AWD values could be compared across time points and evaluated irrespective of the total area of granules that may be present in the particular confocal plane.

To ensure that the granule regions in the plane of the MTOC were representative of the distance of all of the granules throughout the volume of the cell the, AWD calculation was performed using granule volume and three-dimensional reconstructions of cells. Here the *z*-axis measurements of granule regions from the MTOC were included in the MGD calculation by adding $(z - z_i)^2$ to the *x* and *y* coordinates to allow localization of the granule regions relative to the MTOC throughout the reconstruction. Mean AWD values

obtained in the plane of the MTOC versus the volume weighted distances throughout three dimensions were similar (data not shown).

In streaming video, Volocity "Track Objects" function was used to identify individual lytic granules over time and define the velocity, displacement, and displacement rate of their tracks. The total velocity of the lytic granule track was calculated using the initial and final position of the lytic granule relative to the MTOC and instantaneous velocity was calculated as the slope of the lytic granule track over the continuous minus-end–directed portion of a lytic granule track. To calculate instantaneous velocity, minus-ended movement was arbitrarily defined as at least 1 μm and was considered to have stopped when three consecutive time points showed no MTOC-directed movement.

Fixed cell images (dynein experiment) were analyzed for colocalization of dynein and perforin. In three individual experiments, 5–20 images of each condition were acquired, and from these 37–64 cells in which the MTOC, perforin, and dynein was present were identified and colocalization coefficients determined using Volocity software.

Inhibitors

Where applicable, YTS cells were preincubated with 10 μM paclitaxel (Sigma-Aldrich), 10 μM nocodazole (Sigma-Aldrich), 5 μM cytochalasin D (MP Biomedicals, Solon, OH), or 10 μM latrunculin A (Sigma-Aldrich) for 30 min and then washed. These inhibitors were also added during imaging of inhibitor pretreated cells.

Nucleofection Assays

Isolated eNK cells were nucleofected with the enhanced GFP (EGFP)-tubulin expressing vector using an Amaxa Nucleofector; program O-017, and the human cell reagent (Amaxa, Gaithersburg, MD). Nucleofected cells were incubated in RPMI medium supplemented with 20% FCS overnight before use. GFP-fused p50 dynamitin or CC1 subunit of $p150^{Glued}$ constructs in pEGFP-N1 vector (LaMonte *et al.,* 2002; Ligon *et al.,* 2003) were nucleofected into 1×10^7 YTS cells using program O-017 with reagent R after which cells were cultured for 24 h.

Lytic Granule Isolation and Analysis

Lytic granules were isolated from disrupted YTS cells and used for either mass spectrometry or Western blot analysis, performed as previously described (Sanborn *et al.,* 2009). Western blot analysis using lytic granules and other cellular fractions for identification of dynein complex members was performed as described elsewhere (LaMonte *et al.,* 2002).

Statistical Analysis

The minimum number of cells evaluated was determined using sample size calculations based on preliminary data, with α and β error levels of 1%. Differences between nonactivated and activated NK cells were evaluated using unpaired two-tailed Student's t tests.

RESULTS

MTOC Polarization Occurs Slowly and Only in Cytolytic Conjugates

NK cell cytotoxicity is a stepwise process relying on checkpoints that govern subcellular reorganization culminating in directed secretion to facilitate destruction of a target cell (Wulfing *et al.,* 2003). One critical checkpoint in the cytolytic process is the polarization of the MTOC and lytic granules to the IS so that the lytic granule contents can be secreted. Because NK cells are cytotoxic lymphocytes of the innate immune system with important roles in routine immune surveillance, we hypothesized that the process of MTOC polarization would be gradual, providing ample opportunity for regulation. Thus, we initially evaluated the kinetics of MTOC polarization toward the NK cell IS in real time using immortalized NK cell lines, YTS and NK92, stably expressing GFP-tubulin. Because MTOC polarization is also required for lytic granule reorientation to the IS, NK cells were loaded with LysoTracker Red dye to enable their visualization during the process of MTOC movement.

GFP-tubulin, LysoTracker-loaded YTS or NK92 cells were added to live cell imaging chambers to which target cells were immobilized using specific antibodies. The 721.221 B lymphoblastoid cell line and K562 erythroleukemic cell line were used as target cells for YTS and NK92 cells, respectively, in order to enable formation of cytolytic conjugates which can give rise to cytotoxicity (Figure S1). K562 and YTS cells were also evaluated as examples of noncytolytic conjugates, which do not give rise to cytotoxicity, because YTS cells do not kill K562 cells (Supplemental Figure S1). NK cells contacting target cells were identified and imaged every 15 s within a single z-axis plane containing the MTOC for a minimum of 30 min. The MTOC was identified as a solitary intense cluster of GFP-tubulin, which corresponded to the MTOC as defined by pericentrin localization (Figure 1A). In cytolytic conjugates between either YTS and 721.221 cells (Figure 1B; Supplemental Video 1), or NK92 and K562 cells (Figure 1C; Supplemental Video 2), the MTOC gradually tracked toward the IS. In contrast, in noncytolytic conjugates between YTS and K562 cells, this gradual directed movement was not observed (Figure 1D; Supplemental Video 3). To quantify the kinetics of MTOC movement, the distance between the MTOC and the center of the IS (defined as the center of the interface between the NK and target cell) was measured at each time point. The mean MTOC polarization time to the IS was 35.45 ± 5.73 min in YTS cells and 36.19 ± 2.38 min in NK92 cells (Figure 1, E and F). In contrast, MTOC polarization did not occur in noncytolytic conjugates and the MTOC-to-IS distance remained constant (Figure 1G). Thus, MTOC polarization was specific to the cytolytic IS and occurred gradually.

Lytic Granules Converge to the MTOC Rapidly and before Polarization

Microtubules and the MTOC are required for lytic granule delivery to the IS (Orange *et al.,* 2003), with the MTOC directing the final steps in lytic granules joining the cell membrane (Stinchcombe *et al.,* 2006). The relationship of the lytic granules to the MTOC before its final polarization to the IS, however, is unclear. Although the MTOC was found to gradually track to the IS, the lytic granules were noted to be gathered around the MTOC in newly formed cytolytic conjugates. In these initial experiments, imaging began 1–4 min after cytolytic conjugate formation, and lytic granules were found to be in close proximity to the MTOC either at the outset of imaging or soon afterward (Figure 2, A and B). In time-lapse images, once lytic granules converged to the MTOC, they appeared sustained in this conformation as the MTOC polarized to the IS. The converging of lytic granules was independent of cytolytic activation, or MTOC polarization, because it was also found in noncytolytic conjugates soon after their formation (Figure 2C). Thus, we hypothesized that lytic granules first cluster to the MTOC in order to be delivered with it to the IS.

To objectively define lytic granule movement relative to the MTOC, equations were developed to define the MTOC to granule distance. Specifically, the x, y coordinates of the centroid of each lytic granule within the plane of the MTOC was related to the centroid of the MTOC. The mean value was determined for all lytic granules within the plane of the MTOC of a single NK cell at each individual time point. Compared with distances in unconjugated YTS and NK92 cells, the average distance of granules from the MTOC in the plane of the MTOC over all time points was reduced at least twofold in conjugated cells (Figure 2D). Even in the absence of MTOC polarization, in YTS noncytolytic conjugates, there was a reduction in the distance of the lytic granules from the MTOC over all time points, similar to that in cytolytic conjugates. In either cytolytic or noncytolytic conjugates, differences in the mean distance of lytic granules from the MTOC were not identified once they had converged to the MTOC. Thus, lytic granules remained converged around

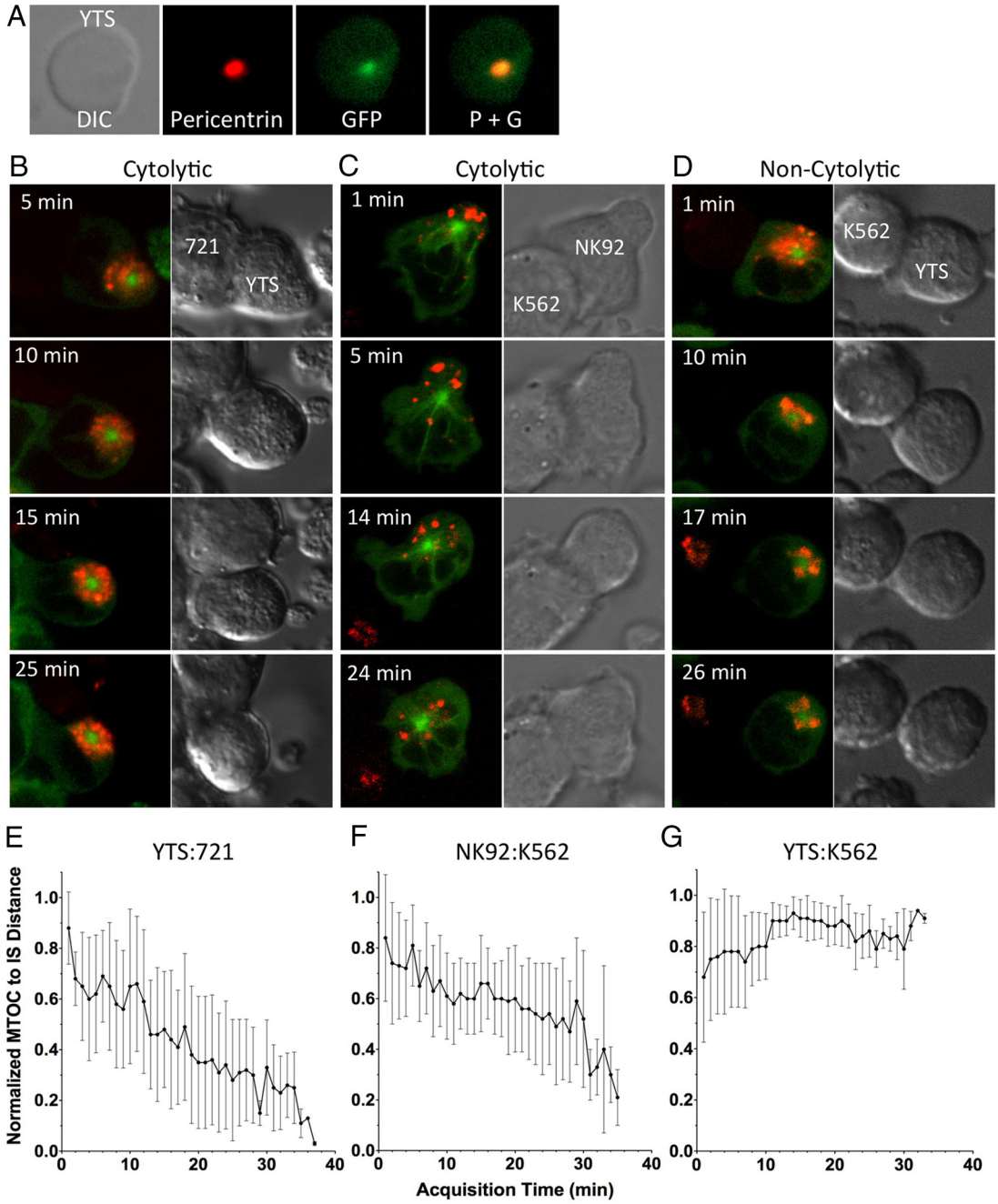

Figure 1. Dynamics of MTOC movement relative to the NK cell IS. (A) DIC (left) and overlay of fluorescent images (right) of a YTS GFP-tubulin cell fixed and stained with anti-pericentrin polyclonal antibody are shown. Green, GFP-tubulin; red, pericentrin antibody as identified using an AlexaFluor-conjugated anti-rabbit mAb. (B–D) Time-lapse images of MTOC movement in a YTS GFP-tubulin cell conjugated with a susceptible 721.221 target cell (B; from Supplemental Video 1), an NK92 GFP-tubulin cell conjugated with a susceptible K562 target cell (C; from Supplemental Video 2), and a YTS GFP-tubulin cell conjugated with a nonsusceptible K562 target cell (D; from Supplemental Video 3). Each image pair shows confocal immunofluorescence in the plane of the MTOC on the left and DIC on the right. Green, GFP-tubulin; red, LysoTracker–loaded acidified lysosomes. Mean distance between the MTOC and the IS (error bars, ±SD), normalized to the largest distance of the MTOC from the IS in that cell, as a function of conjugation time in (E) YTS with 721.221 cells (n = 10), (F) NK92 with K562 cells (n = 9), and (G) YTS with K562 cells (n = 10).

the MTOC throughout conjugation whether the MTOC was polarized or not.

A simple measure of lytic granule to MTOC distance, however, did not account for groups of granules that could not be resolved individually using confocal microscopy. Thus, an equation was developed to give additional weight to lytic granule groupings; area-weighted distance (AWD). Using this equation over all time points, the same trends of lytic granules being clustered to the MTOC in the plane of the MTOC after NK cell conjugation were identified (Supplemental Figure S2A). Thus, lytic granules were accumulated around the MTOC, were sustained in that position, and were independent of cytotoxicity triggering signals.

The measurements thus far also did not take into account any cell spreading that might occur during the course of the experiments, which could bias measurements by pulling

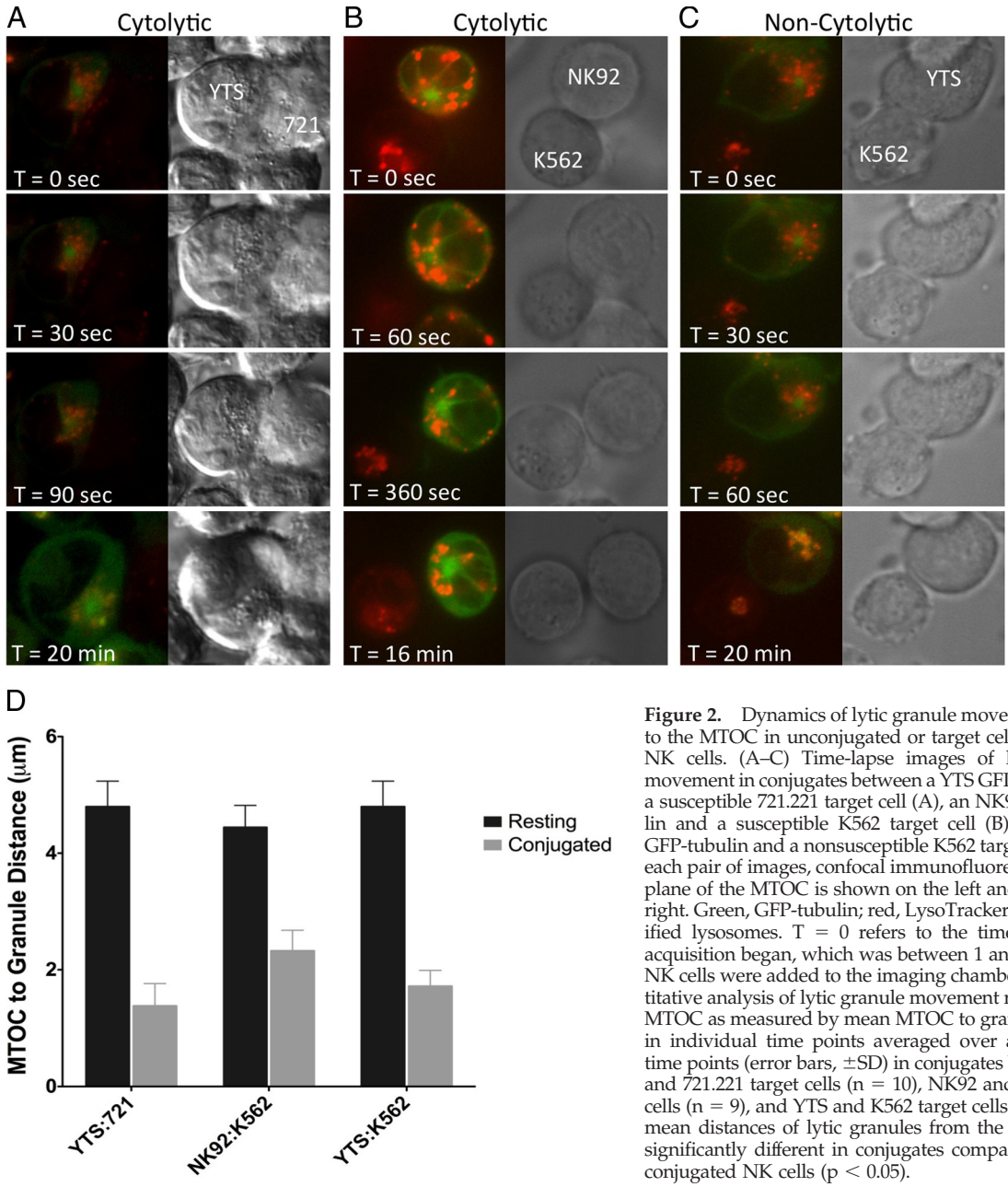

Figure 2. Dynamics of lytic granule movement relative to the MTOC in unconjugated or target cell–conjugated NK cells. (A–C) Time-lapse images of lytic granule movement in conjugates between a YTS GFP-tubulin and a susceptible 721.221 target cell (A), an NK92 GFP-tubulin and a susceptible K562 target cell (B), and a YTS GFP-tubulin and a nonsusceptible K562 target cell (C). In each pair of images, confocal immunofluorescence in the plane of the MTOC is shown on the left and DIC on the right. Green, GFP-tubulin; red, LysoTracker-loaded acidified lysosomes. T = 0 refers to the time that image acquisition began, which was between 1 and 5 min after NK cells were added to the imaging chamber. (D) Quantitative analysis of lytic granule movement relative to the MTOC as measured by mean MTOC to granule distance in individual time points averaged over all measured time points (error bars, ±SD) in conjugates between YTS and 721.221 target cells (n = 10), NK92 and K562 target cells (n = 9), and YTS and K562 target cells (n = 10). All mean distances of lytic granules from the MTOC were significantly different in conjugates compared with unconjugated NK cells ($p < 0.05$).

granules in the direction of the cell footprint. When specifically measured, however, the mean cell perimeter at individual time points did not substantively change over all time points (Supplemental Figure S3A). Thus, it is unlikely that granule movements were a feature of global cell expansion or contraction. The measurements could also be affected by changes in the total lytic granule area in an *x, y* plane. Thus, total lytic granule area was measured in the *x, y* plane of the MTOC in all time points and the mean value did not vary consistently over time (Supplemental Figure S4A). These consistencies were also observed for the other NK cells measured throughout this work (Supplemental Figures S3, B–D, and S4, B–E).

Finally, because the lytic granules in live cells were visualized using LysoTracker-loaded NK cells, an additional method of visualizing lytic granules was pursued to allow for confirmation of measurements of convergence. Here, YTS cells were either left unconjugated, or conjugated to 721.221 target cells, followed by fixation and staining for perforin and tubulin to parallel the live cell experiments and enable detection of the lytic granules and MTOC, respectively. In unconjugated cells the perforin-defined lytic granules were diffusely localized relative to the MTOC, whereas in cells that had been conjugated to a target cell for 5 or 30 min the lytic granules were converged to the MTOC (Supplemental Figure S5A). This was confirmed in repeated experiments using the measurements for the mean distance or AWD of lytic granule regions from MTOC described above, even though the total area of perforin-defined lytic granules was slightly less than that identified by LysoTracker labeling of live cells (Supplemental Figure S5, B–D).

NK Cell Activation Receptors Trigger Rapid Lytic Granule Convergence to the MTOC

The convergence of lytic granules to the MTOC in noncytolytic conjugates suggested that adhesion events alone could

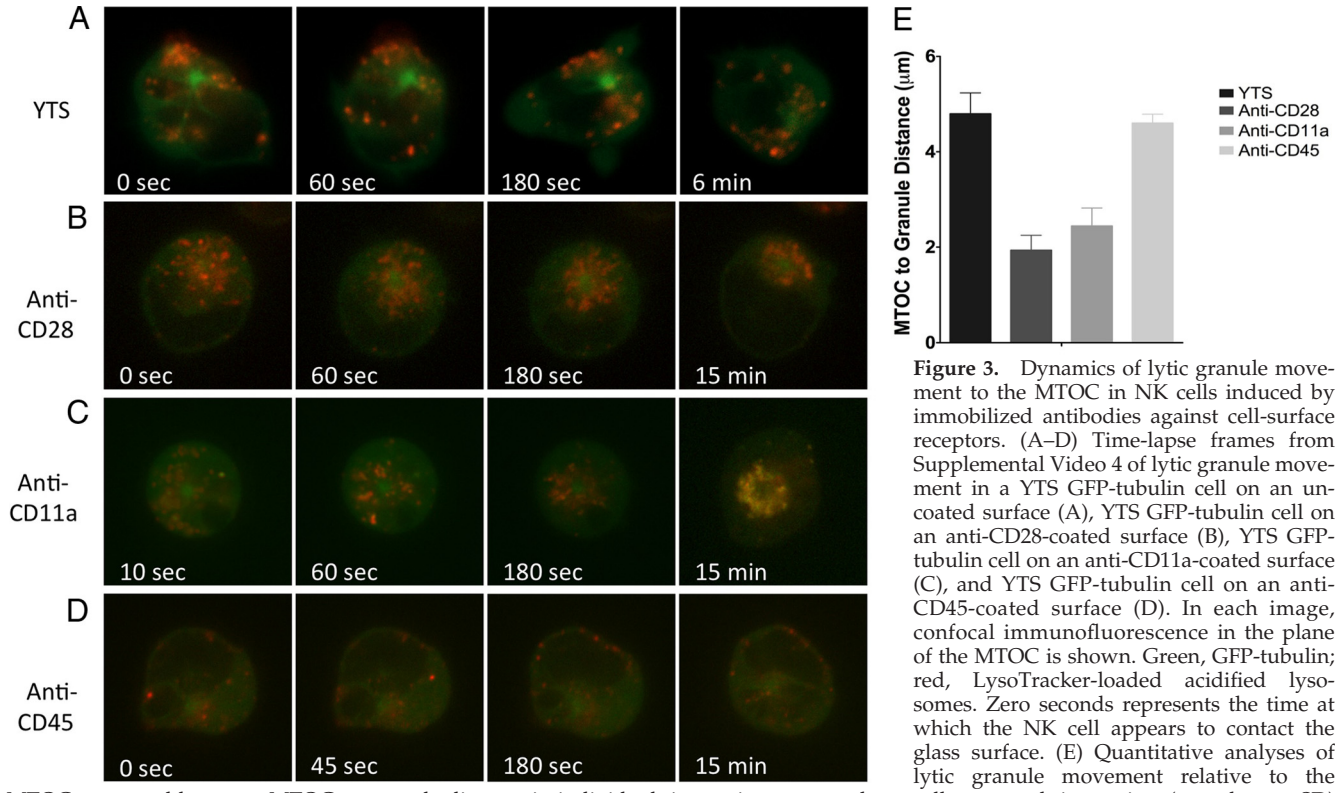

Figure 3. Dynamics of lytic granule movement to the MTOC in NK cells induced by immobilized antibodies against cell-surface receptors. (A–D) Time-lapse frames from Supplemental Video 4 of lytic granule movement in a YTS GFP-tubulin cell on an uncoated surface (A), YTS GFP-tubulin cell on an anti-CD28-coated surface (B), YTS GFP-tubulin cell on an anti-CD11a-coated surface (C), and YTS GFP-tubulin cell on an anti-CD45-coated surface (D). In each image, confocal immunofluorescence in the plane of the MTOC is shown. Green, GFP-tubulin; red, LysoTracker-loaded acidified lysosomes. Zero seconds represents the time at which the NK cell appears to contact the glass surface. (E) Quantitative analyses of lytic granule movement relative to the MTOC measured by mean MTOC to granule distance in individual time points averaged over all measured time points (error bars, ±SD) in 9–10 YTS cells per condition. Mean distances of lytic granules from the MTOC in NK cells on anti-CD28– and anti-CD11a– but not anti-CD45–coated surfaces were significantly different from unconjugated NK cells ($p < 0.05$).

trigger granule motility. To evaluate the activity of isolated receptors, live cell chamber slides were coated with monoclonal antibodies specific for the CD28 lytic receptor, CD11a, or CD45 as a nonactivating receptor, and cells were imaged every 10 s after they contacted the glass surface. When slides were not coated with antibody, the lytic granules remained diffusely localized relative to the MTOC (Figure 3A). After contacting a surface coated with antibody against CD28 or CD11a, however, rapid lytic granule convergence to the MTOC was observed (Figure 3, B and C; and Supplemental Video 4, left and center). YTS cells deposited on surfaces coated with antibody against CD45 adhered, but lytic granules did not converge to the MTOC and remained diffusely localized (Figure 3D; Supplemental Video 4, right).

The distances of the lytic granules to the MTOC in these settings were measured directly (Figure 3E) and with weighting for lytic granule region area (Supplemental Figure S2B). The mean distance of granules from the MTOC over all time points was decreased more than twofold in cells on anti-CD28– or anti-CD11a–coated surfaces when compared with YTS cells in uncoated chambers. The mean distance of granules from the MTOC over time in YTS cells on the anti-CD45–coated surfaces, however, was not different from that in YTS cells in uncoated chambers (Figure 3E). Thus, activating receptors triggered in isolation can specifically induce lytic granule convergence to the MTOC, even if the receptor is not capable of inducing cytotoxicity on its own.

Individual Lytic Granules Rapidly Track toward the MTOC Only after Activation

Although lytic granule movement to the MTOC was implied by the observed clustering around the MTOC at early time points after activation, the individual movements and kinetics of moving granules were not defined. Thus, in order to resolve lytic granule traffic and in an effort to see individual lytic granules moving, rapid fluorescent image acquisition in resting and activated NK cells was performed. In resting YTS or NK92 cells, lytic granules did not move toward the MTOC (images in Figure 4, A and B; Supplemental Videos 5 and 6) and remained stationary. When YTS or NK92 cells were deposited onto chamber slides coated with anti-CD28 or anti-NKp30, respectively, individual granules moved rapidly in short bursts toward the MTOC (images in Figure 4, C and D; Supplemental Videos 7 and 8).

To quantify the lytic granule movements, the distance of each lytic granule from the MTOC was measured at each time point by comparing the *x, y* coordinates of both objects. In resting YTS and NK92 cells, there was negligible change in lytic granule position relative to the MTOC (graphs in Figure 4, A and B). In activated cells, however, lytic granules demonstrated MTOC-directed movement (graphs in Figure 4, C and D). The same paradigm was identified for lytic granules in YTS and NK92 cells conjugated to target cells (Supplemental Figure S6A). The movements of lytic granules in activated NK cells were asynchronous, often abrupt and typically short-lived (Figure 4, C and D). To better gauge directedness of the individual lytic granule tracks, the net velocity of each over its entirety relative to the MTOC was determined. A positive value denoted a net movement toward the MTOC and was found for the mean of all lytic granule tracks in activated cells. These values were significantly different from those in resting NK cells (Figure 4E). The lytic granule velocity over the total run length of individual tracks irrespective of their directionality was also

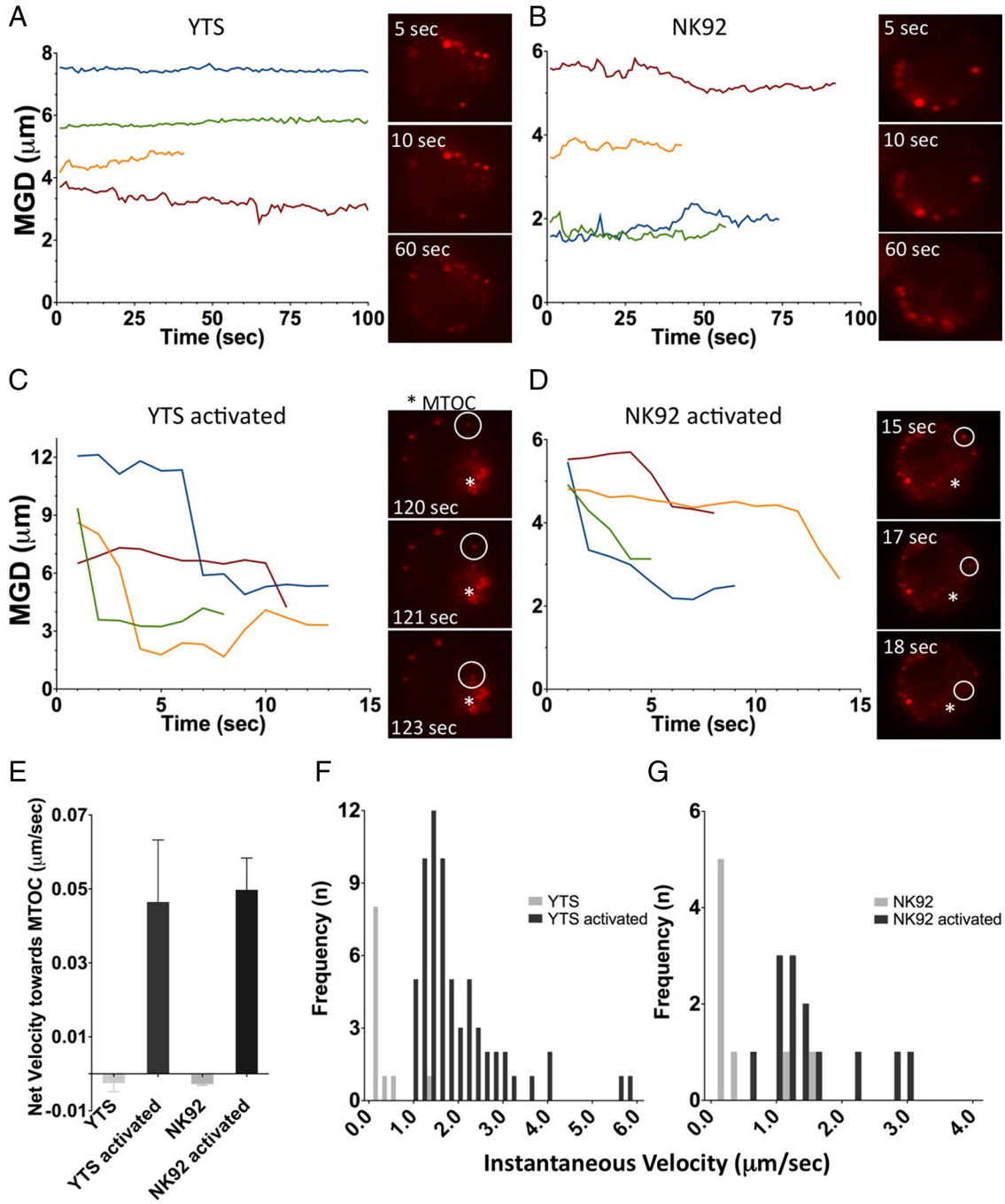

Figure 4. Quantitative analyses of rapid lytic granule movement relative to the MTOC in NK cells. Distance of individual LysoTracker Red–loaded lytic granules from the MTOC as a function of time in a single cell and as visualized in a streaming video sequences in resting YTS GFP-tubulin (A), or NK92 GFP-tubulin (B) cells, and YTS GFP-tubulin cells on an anti-CD28-coated surface (C) or NK92 GFP-tubulin cells on an anti-NKp30–coated surface (D). Times listed in images represent seconds elapsed after the NK cell contacted the glass surface. The MTOC as defined by GFP fluorescent acquisition (not shown) is marked with an asterisk (*), and a white circle tracks an individual moving lytic granule. The line graphs shown each demonstrate four representative single lytic granule tracks, with T = 0 representing the first identification of that granule. In activated NK cells these had a total displacement of >1 μm as did >50% of all granules identified. (E) Mean net velocity of all measured lytic granules over their entire tracks (error bars, ±SD). Each bar represents three cells accounting for 58–141 measured lytic granule tracks; means in activated YTS and NK92 cells were significantly different from resting cells ($p = 0.045$ and $p = 0.0036$, respectively). Histogram of instantaneous velocities of all MTOC-directed lytic granules in YTS GFP-tubulin (F) and NK92 GFP-tubulin cells (G), as they moved toward the MTOC with a displacement of ≥1 μm. Instantaneous velocities in activated YTS and NK92 cells were significantly different from those in resting cells ($p < 0.0001$ and $p = 0.0035$, respectively).

measured and was still greater in activated NK cells (Supplemental Figure S6, B and C). Although the total run length was significantly greater in activated as compared with resting YTS cells, it was not in NK92 cells, and thus the velocity

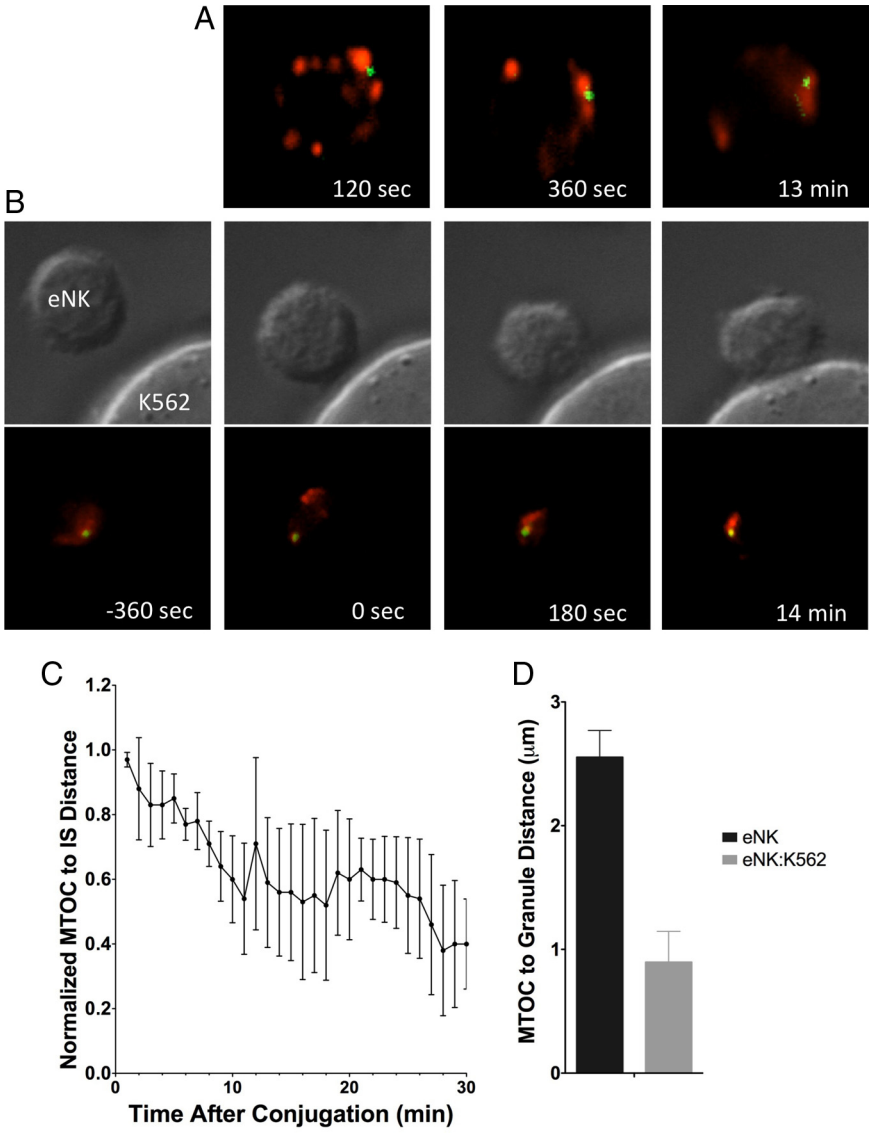

Figure 5. Dynamics of MTOC movement relative to the IS and lytic granule movement relative to the MTOC in unconjugated or target cell–conjugated eNK cells. Time-lapse images of individual eNK cells nucleofected with GFP-tubulin deposited onto an uncoated surface (A) or in conjugation with a susceptible K562 target cell (B; Supplemental Video 9). (B) DIC (top) and confocal immunofluorescence in the plane of the MTOC (bottom). Green, GFP-tubulin; red, LysoTracker-loaded acidified lysosomes. Zero seconds represents the time at which the NK cell appears to contact either the imaging surface or the target cell. (C) Quantitative analyses of mean distance between the MTOC and the IS (error bars, ±SD) normalized to the largest distance of the MTOC from the IS as a function of time. (D) Lytic granule movement relative to the MTOC as a function of time measured by mean MTOC to granule distance in individual time points averaged over all measured time points in nine cells; error bars, ±SD. Mean distance of lytic granules from the MTOC in conjugated eNK cells was significantly different from that in unconjugated eNK cells ($p < 0.05$).

differences cannot be explained by run length alone (Supplemental Figure S6, D and E).

To better quantify abrupt transitions in lytic granule position relative to the MTOC, the instantaneous velocity was determined for only those parts of lytic granule tracks that traveled at least 1 μm in a minus-end–directed manner. Although few lytic granules in resting cells attained this degree of minus-end–directed movement, the instantaneous velocity in activated cells was significantly greater (Figure 4, F and G). The mean instantaneous velocity of lytic granules increased from 0.2 ± 0.4 μm/s in resting to 1.8 ± 1.0 μm/s in activated YTS cells and from 0.4 ± 0.6 μm/s in resting to 1.4 ± 0.7 μm/s in activated NK92 cells. This further demonstrates the directedness of lytic granules to the MTOC after NK cell activation, which occurs soon after the signal is received.

Lytic Granule and MTOC Dynamics in Ex Vivo NK Cells Recapitulate that in NK Cell Lines

Although our findings thus far were established in two distinct NK cell lines, they might not necessarily translate to eNK cells. Thus, to define the observed dynamics of lytic granules and the MTOC as a general characteristic of NK cells, highly enriched eNK cells were prepared from human blood and an α-tubulin-GFP construct introduced immediately after their isolation. Before their conjugation with K562 target cells, eNK cells were incubated with LysoTracker Red dye in order to enable visualization of the lytic granules. In unconjugated eNK cells, a concentration of GFP tubulin signifying the MTOC could be visualized, and lytic granules were diffusely arranged (Figure 5A). In time-lapse images, the lytic granules remained diffuse. Similar lytic granule patterns were observed in eNK cells before conjugation, but soon thereafter, they converged to the MTOC (Figure 5B; Supplemental Video 9) at which point it began to polarize to the IS.

In repeated assays using eNK cells from different donors, the positioning of the MTOC relative to the IS and the lytic granules relative to the MTOC were quantified. The distance of the MTOC from the IS gradually decreased as a feature of conjugation time (Figure 5C). The time required to achieve minimum distance between the MTOC and the IS was also measured in each individual cell and was 22.67 ± 0.29 min. The distance of the lytic granules to the MTOC, however,

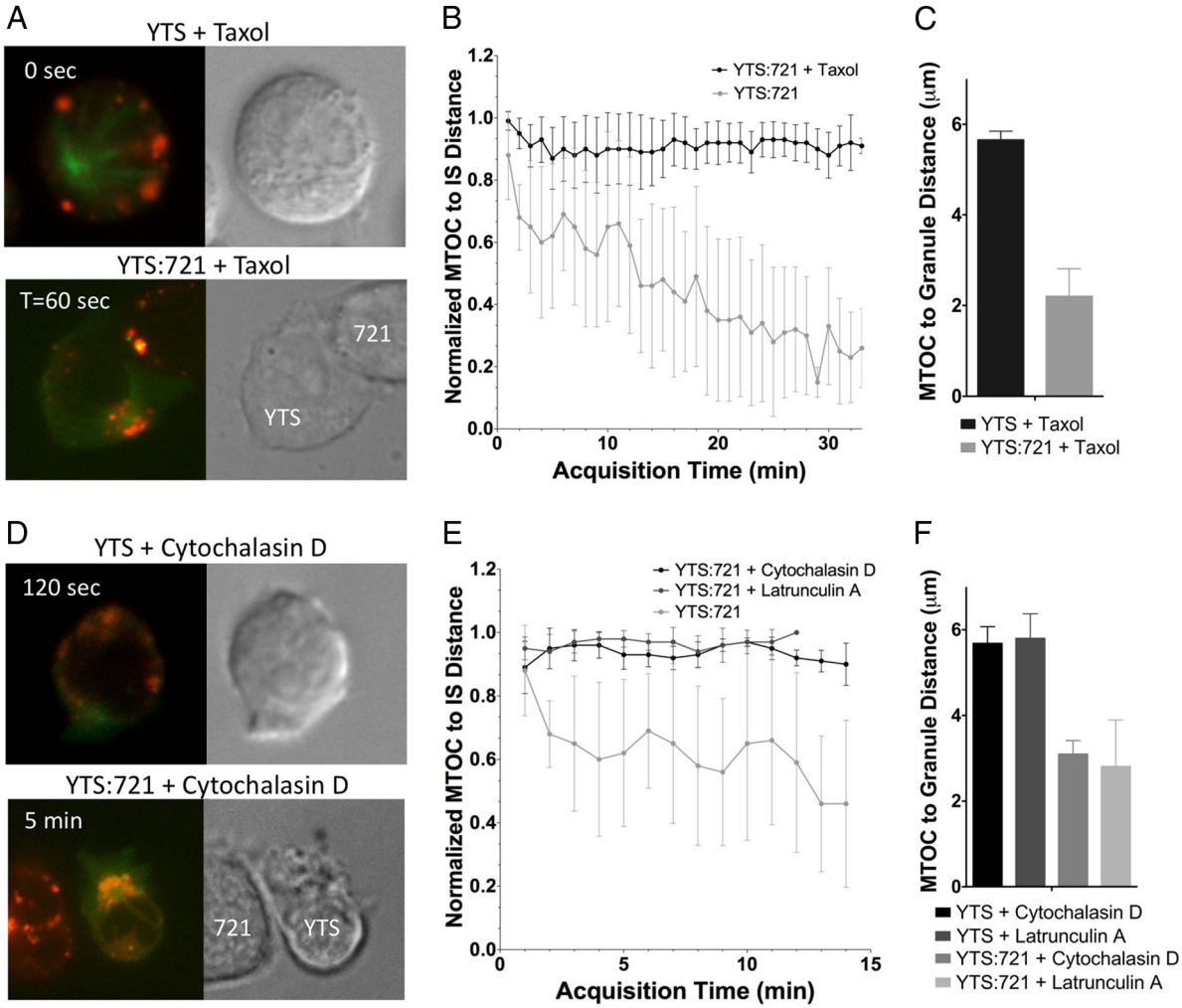

Figure 6. Taxol, cytochalasin D, or latrunculin A treatment does not prevent lytic granule movement to the MTOC in NK cells after target cell conjugation. Images of YTS GFP-tubulin cells treated with taxol (A; Supplemental Video 10) or cytochalasin D (D; Supplemental Video 11) unconjugated or conjugated with a susceptible 721.221 target cell. In each, confocal immunofluorescence in the plane of the MTOC is shown (left; green, GFP-tubulin; red, LysoTracker-loaded acidified lysosomes) and DIC (right). Zero seconds defines the time at which the NK cell appears to contact either the imaging surface or the target cell. (B and E) Quantitative analyses of mean distance (error bars, ±SD) between the MTOC and the IS normalized to the farthest distance of the MTOC from the IS as a function of time in (B) taxol-treated or (E) cytochalasin D– or latrunculin A–treated YTS GFP-tubulin cells conjugated with susceptible 721.221 target cells (n = 10, 8, and 8, respectively). (C and F) Mean MTOC to lytic granule distance in individual time points averaged over all measured time points (error bars, ±SD) in (C) taxol-treated or (F) cytochalasin D– or latrunculin A–treated YTS GFP-tubulin cells conjugated with susceptible 721.221 target cells. Lytic granule distance from the MTOC in drug-treated conjugated NK cells was significantly different from unconjugated drug-treated NK cells ($p < 0.05$).

decreased rapidly when compared with that in unconjugated eNK cells (Figure 5D). At the first time point after target cell contact (6.4 min after acquisition began), the distance of the lytic granules to MTOC had already decreased by 43%. This was substantively before the MTOC was recognized as moving toward the IS, as the MTOC-to-IS distance at these time points was not significantly different from that at T = 0. When the lytic granule regions were weighted according to their area, the rapid convergence to the MTOC was similarly evident (Supplemental Figure S2C) and therefore was not a feature of the relatively small size of eNK cells compared with the cell lines. Thus, the dynamics defined in the NK cell lines reproduces those observed in eNK cells. This likely represents the physiological process by which lytic granules and the MTOC approach the IS, with lytic granules first approximating the MTOC and then the MTOC polarizing to the IS.

Lytic Granule Convergence to the MTOC in Activated NK Cells Occurs Independently of Microtubule and Actin Reorganization

Because lytic granule convergence to the MTOC occurred rapidly after IS formation, we next evaluated the dependence of this MTOC-directed traffic on other known cytoskeletal requirements for IS formation and function. Because microtubule function is required for lytic granule polarization to the IS (Orange *et al.*, 2003), we first asked whether microtubule dynamics and/or MTOC movement was required for lytic granule convergence to the MTOC. Thus, YTS GFP-tubulin cells were treated with Taxol to

stabilize microtubules, incubated with LysoTracker Red dye, and conjugated with target cells (Figure 6A; Supplemental Video 10). Taxol-treated cells still conjugated with target cells, but as would be expected the MTOC failed to polarize to the IS (Figure 6B). Although the lytic granules did not polarize to the IS in Taxol-treated cells, they did continue to rapidly converge to the MTOC after target cell conjugation. This was reflected quantitatively by rapidly decreased MTOC to granule distance (Figure 6C) as well as AWD (Supplemental Figure S2D) when compared with Taxol-treated unconjugated YTS cells. The magnitude and kinetics of lytic granule convergence in the Taxol-treated conjugated cells was not different from that in untreated conjugated cells shown in Figure 2 ($p = 0.17$ and data not shown). Thus, MTOC-directed lytic granule movement occurs independently of microtubule dynamics and can utilize stabilized microtubules to move toward a fixed MTOC.

To define the dependency of lytic granule convergence to the MTOC on microtubules, YTS GFP-tubulin cells were treated with nocodazole before conjugation with target cells. Similar to taxol treatment, the NK cells still conjugated with target cells but because of nocodazole-induced destabilization, the microtubule network and the MTOC were not visualized. In these cells, although there was no MTOC, clustering of lytic granules within the cell was not found (Supplemental Figure S7). Thus, lytic granule convergence in NK cells after activation requires intact microtubules but does not require microtubule dynamics. This suggests specific motor-driven traffic of lytic granules along microtubules to the MTOC rapidly after target cell recognition.

One of the earliest and most rapid events in formation and function of the NK cell IS is the reorganization of F-actin at the IS. It occurs within minutes and is required for activation receptor clustering at and lytic granule polarization to the NK cell IS (Orange *et al.*, 2003). Thus, we next determined if the large-scale actin reorganization required for cytotoxicity was also a requirement for lytic granule convergence to the MTOC. YTS GFP-tubulin cells were treated with cytochalasin D, or latrunculin A before their conjugation with target cells to prevent F-actin reorganization. In cytochalasin D–treated cells, conjugates tended to be short-lived and YTS cells were frequently misshapen (Figure 6D; Supplemental Video 11). As previously demonstrated, with either inhibitor the MTOC did not polarize to the IS (Figure 6E). In contrast, lytic granules converged rapidly to the MTOC after conjugation when compared with cytochalasin D– or latrunculin A–treated unconjugated cells. This was true when measuring either the MTOC to granule distance or AWD (Figure 6F and Supplemental Figure S2D). Thus, despite in some cases forming short-lived contacts and with an inhibited ability to reorganize F-actin, lytic granule convergence still occurred. Lytic granule convergence to the MTOC, therefore, is rapid and independent of previously identified cytoskeletal requirements for IS function.

Lytic Granule Convergence to the MTOC during Synapse Formation Requires LFA-1

Because lytic granule convergence to the MTOC during IS formation is rapid and appears to be independent of many previously identified checkpoints in the process of lytic synapse maturation, we considered the initial adhesion event as one promoting convergence. Although a variety of adhesion mechanisms are utilized by human NK cells, that attributable to LFA-1 is required (Kohl *et al.*, 1984). Furthermore, ligation of LFA-1 has been shown to enable the focusing of lytic granules to the IS under certain circumstances (Bryceson *et al.*, 2005), and signals downstream of LFA-1 in NK cells are independent of F-actin reorganization (Riteau *et al.*, 2003). Thus, we evaluated the role of LFA-1 in lytic granule convergence by tracking lytic granules after the addition of blocking LFA-1 antibody (anti-CD11a) or control IgG. Noncytolytic conjugates between YTS and K562 cells were evaluated in these experiments to allow focus on the signal for convergence without the signal required for cytotoxicity (as would be provided by the 721.221 target cell). In the presence of anti-CD11a antibody only approximately half of conjugates demonstrated an obviously deformed NK cell surface at the IS (Figure 7A). The other half made a sustained contact, but failed to demonstrate obvious surface deformation and are referred to as contacts instead of conjugates (Figure 7B). In either case, the lytic granules failed to converge to the MTOC when compared with IgG control (Figure 7C). The mean MTOC to lytic granule distance was measured across all time points and was not found to be different in conjugates or contacts with anti-CD11a blocking antibody, but both were greater than that measured with control IgG (Figure 7D). Thus, LFA-1 is required for lytic granule convergence to the MTOC in NK cells.

Dynein/Dynactin Activity Traffics Lytic Granules to the MTOC

The ability of lytic granules to move toward the MTOC when microtubules were intact, even when they were stabilized, implies a role for a motor protein in their transport. To identify the motor used by lytic granules, mass spectrometry of purified NK cell lytic granules was performed. Among a list of 644 proteins identified, the only known minus-end–directed motor component was dynein heavy chain (Figure 8A). To confirm this association of dynein with lytic granules and to demonstrate the presence of the dynein/dynactin complex, lytic granules were purified from YTS cells and evaluated by Western blot analysis along with the postnuclear cell lysate and crude lysosomal cell fractions used for lytic granule preparation. The purified lytic granules demonstrated an abundance of granzyme B, as would be expected, and also demonstrated dynein heavy chain, the $p150^{Glued}$ subunit of dynactin, the dynein intermediate chain, and p50 dynamitin (Figure 8B). To determine if dynein was colocalized with lytic granules in intact NK cells, dynein heavy chain was evaluated before and after target cell conjugation by microscopy (Figure 8, C–E). Colocalization between the lytic granule area and dynein was evaluated quantitatively through measurement of colocalization coefficients (Figure 8F). When considering the total visualized dynein or lytic granules, some degree of baseline colocalization between the two was identified. When considering total dynein fluorescence, the colocalization with lytic granules did not change after conjugation. When considering lytic granule regions, however, the colocalization with dynein did increase after conjugation. This could be a feature of lytic granule convergence leading to increased colocalized dynein fluorescent intensity in a unit area or could represent some additional recruitment of dynein to lytic granules. The consistent colocalization coefficient when evaluating total dynein, however, suggests the former.

Dynein works in concert with dynactin to move cargo along microtubules in a processive minus-end–directed manner (Gill *et al.*, 1991; King and Schroer, 2000). Thus, we hypothesized that the dynein/dynactin complex was the motor responsible for lytic granule traffic to the MTOC in NK cells. To evaluate this hypothesis, the function of the dynein/dynactin complex was disrupted by overexpression of either p50 dynamitin or the first coiled coil domain of

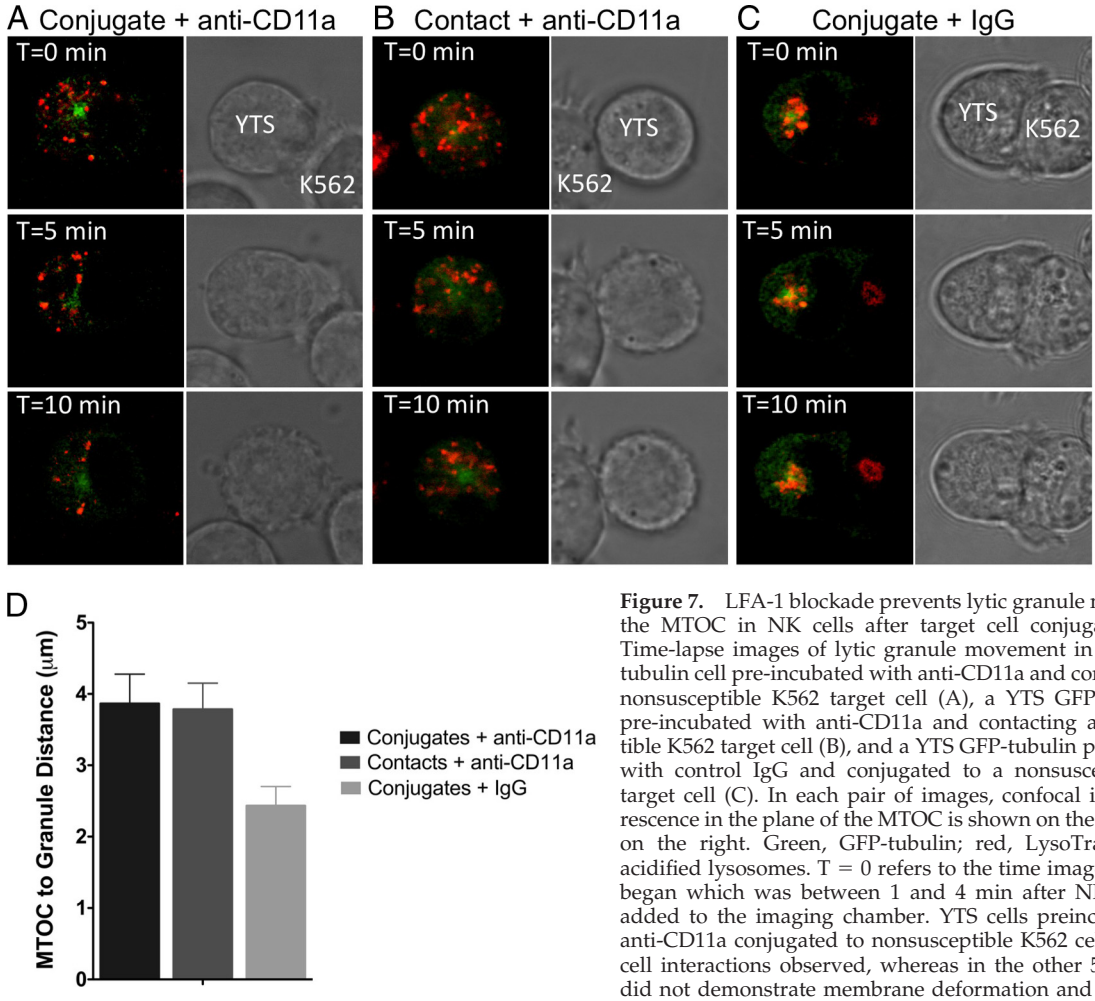

Figure 7. LFA-1 blockade prevents lytic granule movement to the MTOC in NK cells after target cell conjugation. (A–C) Time-lapse images of lytic granule movement in a YTS GFP-tubulin cell pre-incubated with anti-CD11a and conjugated to a nonsusceptible K562 target cell (A), a YTS GFP-tubulin cell pre-incubated with anti-CD11a and contacting a nonsusceptible K562 target cell (B), and a YTS GFP-tubulin pre-incubated with control IgG and conjugated to a nonsusceptible K562 target cell (C). In each pair of images, confocal immunofluorescence in the plane of the MTOC is shown on the left and DIC on the right. Green, GFP-tubulin; red, LysoTracker-loaded acidified lysosomes. T = 0 refers to the time image acquisition began which was between 1 and 4 min after NK cells were added to the imaging chamber. YTS cells preincubated with anti-CD11a conjugated to nonsusceptible K562 cells in 50% of cell interactions observed, whereas in the other 50% the YTS did not demonstrate membrane deformation and are thus described separately as a contact. YTS cells preincubated with IgG routinely conjugated to K562 cells. (D) Quantitative analysis of lytic granule movement relative to the MTOC as measured by mean MTOC to granule distance in individual time points averaged over all measured time points (error bars, ±SD) in conjugates between anti-CD11a–coated YTS and K562 target cells (n = 10), contacts between anti-CD11a–coated YTS and K562 target cells (n = 10), and conjugates between IgG-coated YTS and K562 target cells (n = 5). Mean distances of lytic granules from the MTOC in anti-CD11a–coated YTS cells were significantly greater than in IgG-coated YTS cells ($p < 0.001$).

p150^{Glued} (CC1). Transient expression of these has been previously described to block dynein function (Waterman-Storer *et al.*, 1995; Burkhardt *et al.*, 1997). Thus, p50 or CC1 GFP fusion proteins were expressed in YTS cells. The use of GFP fusion proteins facilitated identification of cells that had received the overexpression constructs and would have reduced dynein function. This however, precluded the use of GFP-tubulin to define the MTOC, and instead the distance of lytic granules from the centroid of the region bounded by all individual lytic granule regions was measured. When cells received a GFP-only construct, lytic granules converged rapidly after target cell conjugation (Figure 9A). In cells receiving either p50-GFP or CC1-GFP, however, lytic granules were localized at the cell periphery and did not move centrally over the course of the experiment (Figure 9, B and C; Supplemental Video 12). To quantify these observations, the lytic granule-to-centroid distance was measured, and mean values calculated for each time point. The mean distance of the lytic granules from their centroid over time was significantly greater in p50- and CC1-overexpressing cells when compared with those expressing GFP only (Figure 9D). The lytic granules in the p50- and CC1-overexpressing cells also demonstrated little movement, as their mean total displacement was only 68 and 66%, respectively, of that recorded in GFP control cells. Thus, lytic granules depend on dynein for their early rapid MTOC-directed movement. This defines dynein and lytic granule convergence to the MTOC as an early prerequisite step required for lytic granule polarization to the NK cell IS, but one that does not commit the NK cell to cytotoxicity. The dynein-dependent MTOC-directed compression of a cargo to enable precise delivery, represents a novel form of directed secretion.

DISCUSSION

NK cell cytotoxicity occurs through a series of highly regulated linear stages enabling maturation and function of the IS (Orange, 2008). Previously, MTOC polarization was defined as a crucial step in delivering lytic granules to the target cell (Stinchcombe *et al.*, 2001, 2006; Wulfing *et al.*, 2003; Banerjee *et al.*, 2007). We have quantified MTOC dynamics and found that in cell lines and ex vivo NK cells polarization occurs gradually and requires lytic triggering (Figures 1 and 5). MTOC polarization did not occur when microtubules were stabilized or when F-actin reorganization was inhib-

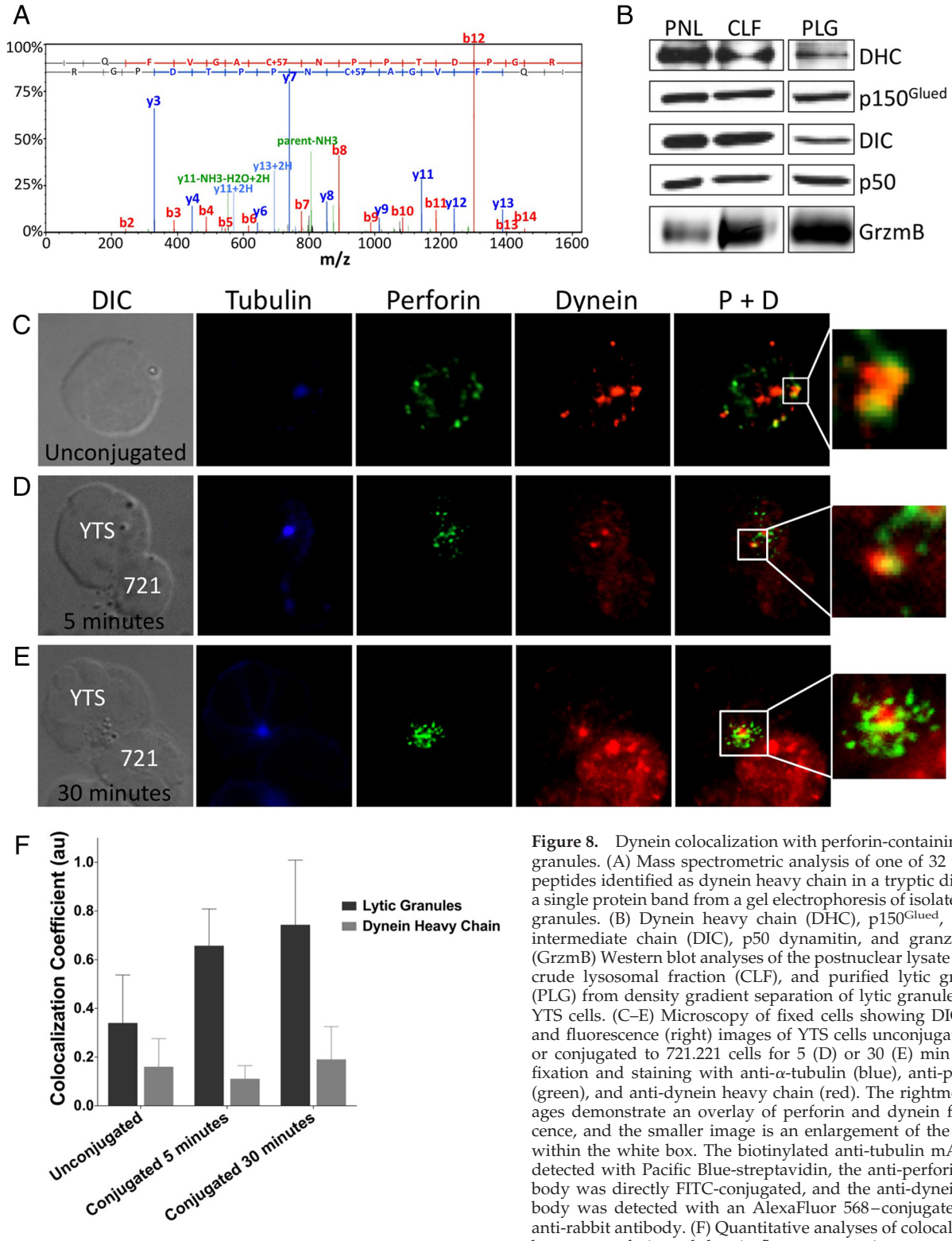

Figure 8. Dynein colocalization with perforin-containing lytic granules. (A) Mass spectrometric analysis of one of 32 unique peptides identified as dynein heavy chain in a tryptic digest of a single protein band from a gel electrophoresis of isolated lytic granules. (B) Dynein heavy chain (DHC), p150^{Glued}, dynein intermediate chain (DIC), p50 dynamitin, and granzyme B (GrzmB) Western blot analyses of the postnuclear lysate (PNL), crude lysosomal fraction (CLF), and purified lytic granules (PLG) from density gradient separation of lytic granules from YTS cells. (C–E) Microscopy of fixed cells showing DIC (left) and fluorescence (right) images of YTS cells unconjugated (C) or conjugated to 721.221 cells for 5 (D) or 30 (E) min before fixation and staining with anti-α-tubulin (blue), anti-perforin (green), and anti-dynein heavy chain (red). The rightmost images demonstrate an overlay of perforin and dynein fluorescence, and the smaller image is an enlargement of the region within the white box. The biotinylated anti-tubulin mAb was detected with Pacific Blue-streptavidin, the anti-perforin antibody was directly FITC-conjugated, and the anti-dynein antibody was detected with an AlexaFluor 568–conjugated goat anti-rabbit antibody. (F) Quantitative analyses of colocalization between perforin and dynein fluorescent regions as measured by the colocalization coefficient between the total cellular lytic granule area (black) or total cellular dynein area (gray) as a feature of conjugation time. Data are representative of three separate repeats in which 37–64 cells were evaluated per condition. Error bars, ±SD.

ited (Figure 6, B and E). Without MTOC polarization, there was no reorientation of lytic granules to the IS. Thus, MTOC polarization is required for the IS-directed dynamics of lytic granules and supports previous data in fixed cytotoxic T-lymphocytes (CTLs), defining this requirement for the MTOC (Stinchcombe *et al.*, 2006; Jenkins *et al.*, 2009). We have previously identified critical regulation of MTOC polarization for cytotoxicity (Banerjee *et al.*, 2007), which is a

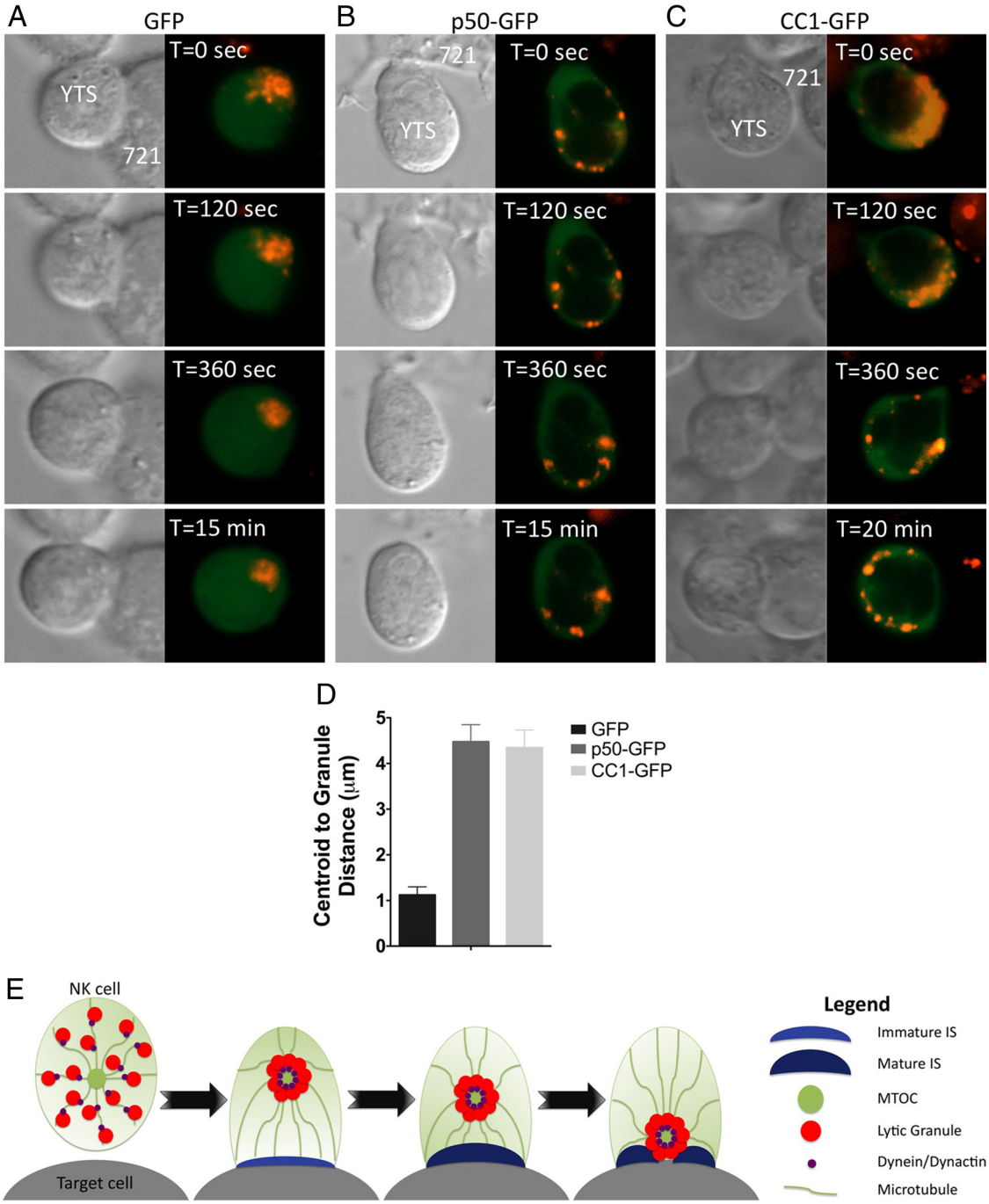

Figure 9. Dynein/dynactin activity is required for rapid lytic granule traffic to the MTOC in NK cells. Time-lapse images of YTS cells nucleofected with GFP (A), p50-GFP (B), or CC1-GFP (C) and in conjugation with susceptible 721.221 target cells (Supplemental Video 12). In each pair of images, confocal immunofluorescence in the plane of lytic granules (left; green, overexpressed GFP fusion protein; red, LysoTracker-loaded acidified lysosomes) and DIC (right) are shown. T = 0 refers to the time acquisition began, which was between 0 and 2 min after the NK cells were added to the imaging chamber. (D) Lytic granule movement relative to the centroid of the granules as measured by mean centroid to granule distance over time (error bars, ±SD) in control GFP-, p50-GFP-, or CC1-GFP–nucleofected YTS cells conjugated with susceptible 721.221 target cells (n = 5). All distances of lytic granules from the granule centroid in p50- or CC1-nucleofected conjugates were significantly greater than those in GFP-nucleofected conjugates ($p < 0.05$). (E) Model of the linear sequence of events leading to directed secretion of lytic granule contents in an NK cell. In the first step, an NK cell recognizes a target cell and the dynein/dynactin complex rapidly transports lytic granules to the MTOC. Next, the lytic granules converge to the MTOC independently of microtubule dynamics or actin reorganization at the IS. Finally, the MTOC gradually polarizes along with the lytic granules to the IS where their contents can be directed onto the target cell.

desirable point for controlling the NK cell IS in light of the lethal nature of the directed secretion of lytic granule contents. The gradual MTOC polarization to the NK cell IS,

however, suggested the existence of other MTOC-related steps prerequisite to function.

The gradual movement of the MTOC was defined in contrast to an unexpected and rapid movement of lytic granules to the MTOC after NK cell activation and before MTOC polarization to the IS. The distance of lytic granules from the MTOC rapidly decreased in NK cells engaged in cytolytic or noncytolytic interactions (Figure 2 and Supplemental Figure S2). This was further explored using immobilized antibodies against specific receptors and those with activating potential (CD28 and CD11a) induced lytic granule convergence compared with nonactivated cells, whereas a nonactivating receptor (CD45) did not (Figure 3). Although CD28 can trigger cytotoxicity in YTS cells (Chen *et al.*, 2006), CD11a can only trigger under certain circumstances (Barber *et al.*, 2004). Thus, granule convergence to the MTOC occurs after some activation, but does not commit the cell to cytotoxicity. This was further demonstrated in noncytolytic conjugates in that CD11a was required for convergence of lytic granules to the MTOC (Figure 7). For this reason it appears that lytic granule convergence is prerequisite to, but not defining of, cytotoxicity in NK cells. In this light, rapid lytic granule convergence may represent a mechanism with which an NK cell prepares itself for cytotoxicity while activation signals are being further integrated. This would serve the purpose of centrally localizing the lytic granules after a successful adhesion event to ensure that they are not secreted until gradual MTOC polarization brings them into proximity with the IS where their contents can be secreted as a targeted bolus. Thus, in a complex tissue lytic granule convergence could protect healthy surrounding cells from cytotoxicity while directing function at the IS formed with a diseased cell.

Lytic granule convergence still occurred even if microtubules were stabilized, or F-actin reorganization was inhibited (Figure 6). This underscores that the MTOC-directed movement of lytic granules is an extremely early event in formation and function of the NK cell lytic IS. Microtubule stabilization defines that MTOC movement is not required for lytic granule convergence and that it can occur before any reorientation to the synapse has been initiated. This identifies MTOC-directed lytic granule movement as an initial step in synapse function relevant to the microtubule network.

Actin accumulation at the IS has been defined to occur rapidly and is required for cell surface receptor clustering and lytic granule polarization as shown using cytochalasin D–treated cells (Orange *et al.*, 2003). Thus, it was surprising that lytic granule convergence still occurred in cells treated with cytochalasin D or latrunculin A. This suggests that signals required for lytic granule convergence, while downstream of activating receptors, are at least partially independent of those requiring significant actin reorganization at the IS. Thus far, few signaling events upstream of F-actin reorganization in NK cells have been defined at a cellular level (Riteau *et al.*, 2003; Butler *et al.*, 2008). These include LFA-1 signaling (Riteau *et al.*, 2003), which was defined as required for granule convergence in noncytolytic conjugates (Figure 7) where the lytic granule convergence was typically present (Figure 2), but the MTOC did not polarize (Figure 1). Thus, the engagement of LFA-1 can represent a minimal, but potentially nonexclusive requirement for lytic granule convergence to the MTOC. Although complete independence from actin reorganization, however, cannot be confirmed with the inhibitor-based experiments presented here, a divergence in signaling would presumably occur after NK cell activation to drive granule convergence. The signal leading to lytic granule convergence would be one that could enable dynein activity and function in granule traffic without needing to promote microtubule or actin reorganization.

Lytic granule convergence to the MTOC was defined initially in our work using the immortalized cell lines YTS or NK92. These are derived from an NK cell lymphoma and leukemia, respectively. Although they are therefore, by definition, abnormal, they both effectively mediate cytotoxicity and form a lytic IS. It was reassuring that these two cell lines derivative from different individuals both demonstrated similar characteristics of lytic granule polarization and convergence. It was still possible, however, that the phenomenon was representative of some baseline cell activation, one that would not be present in vivo under routine conditions of NK cell–mediated immunosurveillance. Thus, NK cells were directly evaluated ex vivo without culture in interleukin-2 or other growth-inducing cytokines (Figure 5). Although this approach presented technical limitations, the lytic granule polarization to the IS and convergence to the MTOC reproduced that found in the cell lines. Thus, without exogenous activation signals, gradual MTOC polarization and rapid lytic granule convergence to the MTOC appear as generalizable phenomena in NK cells.

Characteristics of lytic granules in NK cells may be different from in T-cells, something suggested by previous observations of MTOC movement and Ca^{2+} flux in murine NK cells when compared with murine T-cells (Wulfing *et al.*, 2003). Lytic granules are preformed in the vast majority of human NK cells, which enables the constant ability to kill. This, however, potentially puts the onus of more opportunity for regulation of killing on the NK cell and may relate to the role of NK cells in innate immunity and surveillance versus clonal expansion and the ready effector function of T-cells. The difference in functions is also suggested by the potentially greater strength of signals downstream of the T-cell receptor complex compared with NK cell–activating receptors. T-cell receptor signal strength has been described to dictate the path of lytic granules to specific locations within the IS (Beal *et al.*, 2009). In NK cells, however, lytic granule convergence to the MTOC was found even in noncytolytic interactions (Figure 2), suggesting convergence as an NK cell paradigm for managing granules that may reflect differences between innate and adaptive immunity. Thus, a potentially more regimented control of lytic granules in NK cells may result from a need to manage the abundance of granules present in all mature human NK cells and provide additional checkpoints in cytotoxicity.

Aside from CTLs, other cell types traffic lysosome-related organelles along microtubules in minus-end–directed manner. Lysosomal tracking toward the MTOC has been observed in normal rat kidney cells after interphase, but the specific motors responsible were not defined (Matteoni and Kreis, 1987). Melanosomes in melanocytes are responsive to rapid changes in requirement for distribution of pigment and have also been described to aggregate (Nilsson and Wallin, 1997). Here, kinesins and dynein work in concert to disperse or aggregate pigment, respectively (Nilsson and Wallin, 1997; Nascimento *et al.*, 2003). Minus-end–directed melanosome transport, however, is not a means for directed secretion as it is in NK cells, but serves to aggregate melanosomes at the MTOC to prevent secretion of pigment (Nascimento *et al.*, 2003). The utility of minus-ended microtubule traffic before MTOC reorientation to facilitate directed secretion that we have described is to our knowledge novel and may represent a useful paradigm in generating precision and regulation of secretory function.

In our experiments, the average instantaneous velocity of individual lytic granules was 1.8 μm/s in activated YTS cells and 1.4 μm/s in activated NK92 cells (Figure 4, F and G). This is more rapid than measured velocity of dynein-dependent minus-end–directed movements of melanosomes, which are recorded at 0.25 μm/s (Levi *et al.*, 2006). Very rapid melanosome aggregation to the MTOC (7.4–11.6 μm/s), however, has been identified, although not attributed to dynein specifically (McNamara and Ribeiro, 2000). In other cell types including fibroblasts, normal rat kidney cells, and in *Caenorhabditis elegans* as well as in in vitro assays, minus-ended movements have also been measured at high speeds between 0.7 and 2.5 μm/s (Lye *et al.*, 1987; Matteoni and Kreis, 1987; Schroer and Sheetz, 1991; Presley *et al.*, 1997; King and Schroer, 2000; Toba *et al.*, 2006). Distance traveled by lytic granules was also evaluated (Supplemental Figure S6, D and E) and was found to have run lengths of 4.3 μm on average for activated YTS cells and 2.9 μm on average for NK92 cells. In published results, fluorescent beads or pre-Golgi vesicles have been observed to travel from 1.5–5.0 μm at one time (Presley *et al.*, 1997; King and Schroer, 2000). Thus, in our single granule analyses in streaming videos, the minus-end–directed movement in NK cells was commensurate with that observed in other cell types as well as with dynein motor function.

Lytic granule traffic and dynein function was evaluated in NK cells by overexpression of dynactin components. Dynein processivity requires dynactin for the majority of dynein-dependent cargo transport in cytoplasm (Waterman-Storer *et al.*, 1997). When the p50 subunit is overexpressed, it competitively binds to $p150^{Glued}$ and Arp1, thereby blocking proper binding of dynactin subunits and causing dissolution of the complex (Burkhardt *et al.*, 1997). Overexpression of $p150^{Glued}$ subunits such as CC1 cause dissociation of dynactin from dynein and interruption of function (Waterman-Storer *et al.*, 1995). Using either of these approaches, NK cell lytic granules were found dispersed at the cell periphery (Figure 9). Dynein, therefore, which is associated with lytic granules (Figure 8), is required for this initial step in lytic granule traffic. Other potential minus-end–directed motors exist, specifically among the kinesin14 family (Endres *et al.*, 2006), but these were not identified in our mass spectrometry analysis (data not shown). Dynein has been previously defined at the IS in T-cells and is required for facilitating MTOC polarization (Combs *et al.*, 2006; Martin-Cofreces *et al.*, 2008), but was not evaluated with regards to a cargo-based motor function in those studies. Thus, to our knowledge our work represents the first demonstration of this role for a microtubule minus-end–directed motor in immune cells.

Dynein-dependent, MTOC-directed lytic granule transport represents an early checkpoint in NK cell cytotoxicity and may act as an initial enabling step in NK cell function prerequisite to a commitment to cytotoxicity (Figure 9E). In this way, the NK cell prepares for cytotoxicity after it recognizes a target cell but needs further signals to mature the IS and commit to the cytotoxic event. This sequence also defines a novel paradigm in a linear series of events leading to directed secretion, one in which an actin-independent signal first aggregates organelles to the MTOC. Here, dynein-dependent, minus-ended microtubule transport compresses a cargo before its being relocalized to the point of secretion. This enables a simplistic efficiency mobilizing a cellular resource for a precision function.

ACKNOWLEDGMENTS

The authors acknowledge Drs. Pinaki P. Banerjee (Children's Hospital of Philadelphia) and Kerry Campbell (Fox Chase Cancer Center) for reagents and Linda Monaco-Shawver and Mariko Tokito for technical assistance. This work was supported by National Institutes of Health (NIH) Grant AI067946 (J.S.O.), an NIH National Institute of Allergy and Infectious Diseases research supplement to promote diversity in health-related research (A.N.M.), and NIH grant GM48661 (E.L.H.).

REFERENCES

Andzelm, M. M., Chen, X., Krzewski, K., Orange, J. S., and Strominger, J. L. (2007). Myosin IIA is required for cytolytic granule exocytosis in human NK cells. J. Exp. Med. *204*, 2285–2291.

Banerjee, P. P., Pandey, R., Zheng, R., Suhoski, M. M., Monaco-Shawver, L., and Orange, J. S. (2007). Cdc42-interacting protein-4 functionally links actin and microtubule networks at the cytolytic NK cell immunological synapse. J. Exp. Med. *204*, 2305–2320.

Barber, D. F., Faure, M., and Long, E. O. (2004). LFA-1 contributes an early signal for NK cell cytotoxicity. J. Immunol. *173*, 3653–3659.

Beal, A. M., Anikeeva, N., Varma, R., Cameron, T. O., Vasiliver-Shamis, G., Norris, P. J., Dustin, M. L., and Sykulev, Y. (2009). Kinetics of early T cell receptor signaling regulate the pathway of lytic granule delivery to the secretory domain. Immunity *31*, 632–642.

Bryceson, Y. T., March, M. E., Barber, D. F., Ljunggren, H. G., and Long, E. O. (2005). Cytolytic granule polarization and degranulation controlled by different receptors in resting NK cells. J. Exp. Med. *202*, 1001–1012.

Burkhardt, J. K., Echeverri, C. J., Nilsson, T., and Vallee, R. B. (1997). Overexpression of the dynamitin (p50) subunit of the dynactin complex disrupts dynein-dependent maintenance of membrane organelle distribution. J. Cell Biol. *139*, 469–484.

Burkhardt, J. K., McIlvain, J. M., Jr., Sheetz, M. P., and Argon, Y. (1993). Lytic granules from cytotoxic T cells exhibit kinesin-dependent motility on microtubules in vitro. J. Cell Sci. *104*(Pt 1), 151–162.

Butler, B., Kastendieck, D. H., and Cooper, J. A. (2008). Differently phosphorylated forms of the cortactin homolog HS1 mediate distinct functions in natural killer cells. Nat. Immunol. *9*, 887–897.

Chen, X., Allan, D. S., Krzewski, K., Ge, B., Kopcow, H., and Strominger, J. L. (2006). CD28-stimulated ERK2 phosphorylation is required for polarization of the microtubule organizing center and granules in YTS NK cells. Proc. Natl. Acad. Sci. USA *103*, 10346–10351.

Combs, J., Kim, S. J., Tan, S., Ligon, L. A., Holzbaur, E. L., Kuhn, J., and Poenie, M. (2006). Recruitment of dynein to the Jurkat immunological synapse. Proc. Natl. Acad. Sci. USA *103*, 14883–14888.

Endres, N. F., Yoshioka, C., Milligan, R. A., and Vale, R. D. (2006). A lever-arm rotation drives motility of the minus-end-directed kinesin Ncd. Nature *439*, 875–878.

Gill, S. R., Schroer, T. A., Szilak, I., Steuer, E. R., Sheetz, M. P., and Cleveland, D. W. (1991). Dynactin, a conserved, ubiquitously expressed component of an activator of vesicle motility mediated by cytoplasmic dynein. J. Cell Biol. *115*, 1639–1650.

Gomez, T. S., Kumar, K., Medeiros, R. B., Shimizu, Y., Leibson, P. J., and Billadeau, D. D. (2007). Formins regulate the actin-related protein 2/3 complex-independent polarization of the centrosome to the immunological synapse. Immunity *26*, 177–190.

Jenkins, M. R., Tsun, A., Stinchcombe, J. C., and Griffiths, G. M. (2009). The strength of T cell receptor signal controls the polarization of cytotoxic machinery to the immunological synapse. Immunity *31*, 621–631.

Katz, P., Zaytoun, A. M., and Lee, J. H., Jr. (1982). Mechanisms of human cell-mediated cytotoxicity. III. Dependence of natural killing on microtubule and microfilament integrity. J. Immunol. *129*, 2816–2825.

King, S. J., and Schroer, T. A. (2000). Dynactin increases the processivity of the cytoplasmic dynein motor. Nat. Cell Biol. *2*, 20–24.

Kohl, S., Springer, T. A., Schmalstieg, F. C., Loo, L. S., and Anderson, D. C. (1984). Defective natural killer cytotoxicity and polymorphonuclear leukocyte antibody-dependent cellular cytotoxicity in patients with LFA-1/OKM-1 deficiency. J. Immunol. *133*, 2972–2978.

LaMonte, B. H., Wallace, K. E., Holloway, B. A., Shelly, S. S., Ascano, J., Tokito, M., Van Winkle, T., Howland, D. S., and Holzbaur, E. L. (2002). Disruption of dynein/dynactin inhibits axonal transport in motor neurons causing late-onset progressive degeneration. Neuron *34*, 715–727.

Levi, V., Serpinskaya, A. S., Gratton, E., and Gelfand, V. (2006). Organelle transport along microtubules in *Xenopus* melanophores: evidence for cooperation between multiple motors. Biophys. J. *90*, 318–327.

Ligon, L. A., Shelly, S. S., Tokito, M., and Holzbaur, E. L. (2003). The microtubule plus-end proteins EB1 and dynactin have differential effects on microtubule polymerization. Mol. Biol. Cell *14*, 1405–1417.

Liu, D., Bryceson, Y. T., Meckel, T., Vasiliver-Shamis, G., Dustin, M. L., and Long, E. O. (2009). Integrin-dependent organization and bidirectional vesicular traffic at cytotoxic immune synapses. Immunity *31*, 99–109.

Lye, R. J., Porter, M. E., Scholey, J. M., and McIntosh, J. R. (1987). Identification of a microtubule-based cytoplasmic motor in the nematode *C. elegans*. Cell *51*, 309–318.

Martin-Cofreces, N. B., Robles-Valero, J., Cabrero, J. R., Mittelbrunn, M., Gordon-Alonso, M., Sung, C. H., Alarcon, B., Vazquez, J., and Sanchez-Madrid, F. (2008). MTOC translocation modulates IS formation and controls sustained T cell signaling. J. Cell Biol. *182*, 951–962.

Matteoni, R., and Kreis, T. E. (1987). Translocation and clustering of endosomes and lysosomes depends on microtubules. J. Cell Biol. *105*, 1253–1265.

McNamara, J. C., and Ribeiro, M. R. (2000). The calcium dependence of pigment translocation in freshwater shrimp red ovarian chromatophores. Biol. Bull. *198*, 357–366.

Nascimento, A. A., Roland, J. T., and Gelfand, V. I. (2003). Pigment cells: a model for the study of organelle transport. Annu. Rev. Cell Dev. Biol. *19*, 469–491.

Nilsson, H., and Wallin, M. (1997). Evidence for several roles of dynein in pigment transport in melanophores. Cell Motil. Cytoskelet. *38*, 397–409.

Orange, J. S. (2008). Formation and function of the lytic NK-cell immunological synapse. Nat. Rev. *8*, 713–725.

Orange, J. S., Harris, K. E., Andzelm, M. M., Valter, M. M., Geha, R. S., and Strominger, J. L. (2003). The mature activating natural killer cell immunologic synapse is formed in distinct stages. Proc. Natl. Acad. Sci. USA *100*, 14151–14156.

Pende, D., *et al.* (1999). Identification and molecular characterization of NKp30, a novel triggering receptor involved in natural cytotoxicity mediated by human natural killer cells. J. Exp. Med. *190*, 1505–1516.

Presley, J. F., Cole, N. B., Schroer, T. A., Hirschberg, K., Zaal, K. J., and Lippincott-Schwartz, J. (1997). ER-to-Golgi transport visualized in living cells. Nature *389*, 81–85.

Riteau, B., Barber, D. F., and Long, E. O. (2003). Vav1 phosphorylation is induced by beta2 integrin engagement on natural killer cells upstream of actin cytoskeleton and lipid raft reorganization. J. Exp. Med. *198*, 469–474.

Sanborn, K. B., Rak, G. D., Maru, S. Y., Demers, K., Difeo, A., Martignetti, J. A., Betts, M. R., Favier, R., Banerjee, P. P., and Orange, J. S. (2009). Myosin IIA associates with NK cell lytic granules to enable their interaction with F-actin and function at the immunological synapse. J. Immunol. *182*, 6969–6984.

Sanchez-Madrid, F., Krensky, A. M., Ware, C. F., Robbins, E., Strominger, J. L., Burakoff, S. J., and Springer, T. A. (1982). Three distinct antigens associated with human T-lymphocyte-mediated cytolysis: LFA-1, LFA-2, and LFA-3. Proc. Natl. Acad. Sci. USA *79*, 7489–7493.

Schroer, T. A., and Sheetz, M. P. (1991). Two activators of microtubule-based vesicle transport. J. Cell Biol. *115*, 1309–1318.

Stinchcombe, J. C., Bossi, G., Booth, S., and Griffiths, G. M. (2001). The immunological synapse of CTL contains a secretory domain and membrane bridges. Immunity *15*, 751–761.

Stinchcombe, J. C., Majorovits, E., Bossi, G., Fuller, S., and Griffiths, G. M. (2006). Centrosome polarization delivers secretory granules to the immunological synapse. Nature *443*, 462–465.

Toba, S., Watanabe, T. M., Yamaguchi-Okimoto, L., Toyoshima, Y. Y., and Higuchi, H. (2006). Overlapping hand-over-hand mechanism of single molecular motility of cytoplasmic dynein. Proc. Natl. Acad. Sci. USA *103*, 5741–5745.

Vyas, Y. M., Mehta, K. M., Morgan, M., Maniar, H., Butros, L., Jung, S., Burkhardt, J. K., and Dupont, B. (2001). Spatial organization of signal transduction molecules in the NK cell immune synapses during MHC class I-regulated noncytolytic and cytolytic interactions. J. Immunol. *167*, 4358–4367.

Waterman-Storer, C. M., Karki, S., and Holzbaur, E. L. (1995). The p150Glued component of the dynactin complex binds to both microtubules and the actin-related protein centractin (Arp-1). Proc. Natl. Acad. Sci. USA *92*, 1634–1638.

Waterman-Storer, C. M., Karki, S. B., Kuznetsov, S. A., Tabb, J. S., Weiss, D. G., Langford, G. M., and Holzbaur, E. L. (1997). The interaction between cytoplasmic dynein and dynactin is required for fast axonal transport. Proc. Natl. Acad. Sci. USA *94*, 12180–12185.

Wulfing, C., Purtic, B., Klem, J., and Schatzle, J. D. (2003). Stepwise cytoskeletal polarization as a series of checkpoints in innate but not adaptive cytolytic killing. Proc. Natl. Acad. Sci. USA *100*, 7767–7772.